# Direct Images of the Virtual Source in a Supersonic Expansion†

**Thomas Reisinger,* Gianangelo Bracco,‡ Stefan Rehbein,§ Günter Schmahl,|| Wolfgang E. Ernst, and Bodil Holst⊥**

*Graz University of Technology, Institute for Experimental Physics, Petersgasse 16, 8010 Graz, Austria*

*Received: July 31, 2007; In Final Form: September 26, 2007*

Direct images of the virtual source in a supersonic expansion of helium are presented. The images were obtained using a Fresnel zone plate with free-standing zones, 540 $\mu$m in diameter and with an outermost zone width of 50 nm. The general method can be extended to other beams, including seeded beams. Measurements were carried out at absolute source pressures ranging from 11 to 171 bar using a 10 $\mu$m nozzle with a source temperature of 320 K. The size of the virtual source was found to be strongly dependent on pressure, changing from a diameter of 67 ± 6 $\mu$m at an absolute nozzle pressure of 11 bar to 180 ± 9 $\mu$m at 171 bar. The virtual-source brightness displays a maximum at an absolute nozzle pressure of around 30 bar. This phenomenon occurs because of two competing effects: As the pressure increases, the total flux also increases, but at the same time the virtual source broadens. We modeled the expansion process by calculating the velocity distribution with solutions from the Boltzmann equation to estimate the location of the quitting surface where the frequency of interatomic collisions is assumed negligible. Realistic potentials have been used to calculate the cross section for atomic collisions and, for the velocity distribution perpendicular to the center streamline, a proper scaling with distance derived from the continuum expansion model has been introduced. A good agreement between experiments and model has been found and we discuss its approximation limits. For instance, backscattering effects are not included in the calculations and at present we cannot exclude that they also contribute to a broadening of the virtual-source size for the highest pressure regime. The results presented here are important for improving the understanding of the supersonic expansion process. The experimental method might eventually be used as a new way to test molecular and atomic interaction potentials.

## 1. Introduction

Supersonic molecular beam experiments have provided important contributions to various areas of science over the last decades, see for example refs 1−6. Contributions range from molecular interaction, clusters, and spectroscopy experiments to surface and nanoscience. Supersonic molecular beams can be created with neutral atoms at low (thermal) energy, which makes them particularly suited for the investigation of fragile surface structures and insulating materials[7,8] that are difficult to investigate with other methods. They are also useful for surface dynamics experiments because they can probe millielectronvolt as well as microelectronvolt [9−11] energy ranges. Recent new developments include measurements with extreme grazing incidence exploring quantum scattering effects,[12] He-spin echo,[13] and scanning helium microscopy.[14−16]

In a supersonic expansion the mean free path of the atoms is small compared to the nozzle diameter so that the gas leaves the nozzle in the continuum flow regime. After a distance of a few nozzle diameters, the streamlines become straight lines,[17] which can be traced back to one point, the so-called virtual-source point (see Figure 1). As the beam expands, the density, and hence the collision frequency, decrease and eventually a molecular flow regime is reached in which the atoms travel in straight trajectories without further collisions. The onset of the molecular flow regime is often modeled by a so-called quitting surface (see section 3 for more details). When the molecular flow regime (the quitting surface) is reached, the individual trajectories can be traced back to a plane perpendicular to the beam direction of travel and containing the virtual-source point. In this plane a spatial distribution function, which was labeled the virtual source by Beijerinck and Verster,[18] is obtained as shown in Figure 1. The spatial distribution function is most narrow there.

As illustrated in Figure 1 the shape of the virtual-source is determined by the velocity distribution (temperature) of the beam. This is commonly expressed in literature as two temperatures: the temperature of the beam along the direction of travel, $T_{\|}$, and perpendicular to the direction of travel, $T_{\perp}$. The velocity distribution spread of the beam along the direction of travel, $\Delta v_{\|} = \sqrt{2k_B T_{\|}/m}$, with $m$ the atomic mass and $k_B$ the Boltzmann constant, is crucial for accurate diffraction and time-of-flight experiments[19] and a substantial amount of work has therefore been done investigating and modeling the parallel beam temperature.[20−22] Up till now a sufficient angular resolution could be achieved through simple spatial collimation of the beam and the perpendicular velocity distribution, $\Delta v_{\perp} = \sqrt{2k_B T_{\perp}/m}$, has therefore been much less investigated. Theoretical and experimental work was done by Beijerinck et al. in

† Part of the "Giacinto Scoles Festschrift".

* Corresponding author. E-mail treisinger@gmail.com.

‡ CNR-IMEM, Department of Physics, University of Genova, V. Dodecanesco 33, 16146 Genova, Italy.

§ BESSY m.b.H., Albert-Einstein-Strasse 15, 12489 Berlin, Germany.

|| University of Göttingen, Institute for X-ray Physics, Friedrich-Hund-Platz 1, 37077 Göttingen, Germany.

⊥ Present Address: University of Bergen, Department of Physics and Technology, Allegaten 55, 5007 Bergen, Norway.

10.1021/jp076102u CCC: $37.00 
Published on Web 11/07/2007

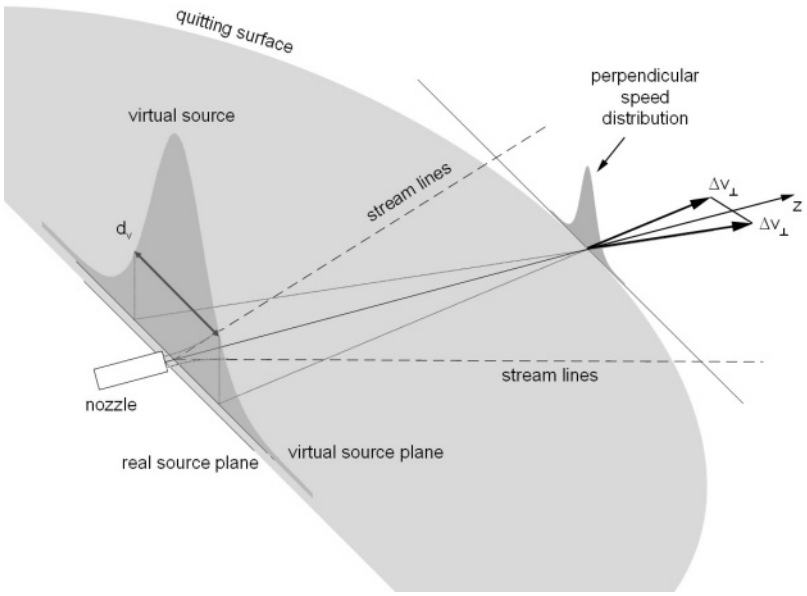


**Figure 1.** Schematic representation of a supersonic expansion and definition of the virtual source. The nozzle expansion can be described as a continuum flow that is axisymmetric about the *z*-axis. Stream lines follow a curved path initially, but after a distance of a few nozzle diameters they become straight and can be traced back to one point, the so-called virtual-source point. The density and hence the collision frequency decrease during the expansion until a molecular flow regime is reached where atoms travel in straight trajectories without further collisions. The transition between the continuum and molecular flow regime occurs at the so-called quitting surface, where it is assumed that collisions stop completely. At the quitting surface, the individual trajectories can be projected backward onto the plane perpendicular to the beam direction of travel that contains the virtual-source point. Taking into account also the width of the distribution of velocities perpendicular to the streamlines $\Delta v_\perp$, one obtains a spatial distribution function that is the virtual source.

the 1980s.[17,18,23,24] Their experiments were carried out with low source pressures and large nozzles (20 $\mu$m or more), stepping across the expanding beam with a narrow slit. The publications by Beijerinck and co-workers remained nearly the only work on the perpendicular temperature for more than a decade until last year when new measurements were presented by DePonte et al.[25] They obtained information on the virtual source using a 2 $\mu$m slit aperture placed 101 mm from the nozzle as a 1-D pinhole camera.

New experimental developments in molecular beam experiments put new demands on the molecular beam sources in terms of such parameters as intensity and coherence. The development of an optimized coherent molecular source requires a detailed knowledge not only of the parallel but also of the perpendicular velocity distribution. For this reason we have investigated experimentally the size of the virtual source of a He beam at different stagnation pressures by using an atom optical element, a Fresnel zone plate, to image the virtual source. A theoretical model has been developed and good agreement is found with the experimental results as well as with recent results from DePonte et al.[25]

## 2. Experimental Apparatus

The experiments presented here were carried out in a molecular beam apparatus named MAGIE. For a detailed description of the apparatus see ref 26. Figure 2 shows a diagram of the experimental setup. A neutral, ground state helium beam is created by a supersonic expansion from a 10 $\mu$m diameter nozzle. The source chamber is pumped by a 3200 L/s (for helium) turbomolecular pump. Measurements were made at source pressures ranging from 11 to 191 bar. The source temperature was kept at 320 K for all experiments, corresponding to an average beam velocity of 1865 m/s and a wavelength of 0.53 Å. The average velocity, $v$, and speed ratio, $S$, of the beam were determined from time-of-flight (TOF) measurements using a double slit chopper (not shown in the diagram in Figure 2). The speed ratio is calculated from $S = 2\sqrt{\ln 2}v/\Delta v$ (where $\Delta v$ is the full width at half-maximum (FWHM) of the measured velocity distribution).[2] The speed ratio varied from 17.5 $\pm$ 5 at 11 bar to 139 $\pm$ 5 at 171 bar, corresponding to a spread in wavelength of 0.051 Å at 11 bar to 0.006 Å at 171 bar. The beam passes through a skimmer, 400 $\mu$m in diameter. Preliminary experiments in our lab had shown that this is significantly larger than the virtual source for the pressure regime here examined. A Fresnel zone plate was placed in the beam line so that the virtual source was in the object plane and a vertical slit/pinhole in the image plane (see Figure 2). The ideal zone plate consists of a set of free-standing concentric rings blocking every other Fresnel zone. The experiment was carried out using a "state of the art" zone plate with a diameter of 540 $\mu$m consisting of 2700 free-standing zones. A detailed description of the fabrication process can be found in ref 27. The zone plate is made of nickel and sits on an underlying Si membrane with a central hole. The central part of the zone plate (the inner 240 zones) was covered by a circular stop (162 $\mu$m in diameter) as part of the fabrication process. This was done to block near the beam center line the zeroth-order part of the diffracted beam as illustrated in the diagram in Figure 2. The zone widths range from 165 nm at the outer rim of the circular stop to 50 nm for the outermost zones. The rings are kept in place by radial support strips.

When reaching the zone plate, the atoms are in the molecular flow regime, traveling in straight lines and not interacting with each other so that the situation is analogous to classical optics. The virtual source was scanned by stepping the vertical slit/pinhole across the image in one or two dimensions. The transmitted signal was measured using an electron bombardment detector. Measurements were performed with two zone plates

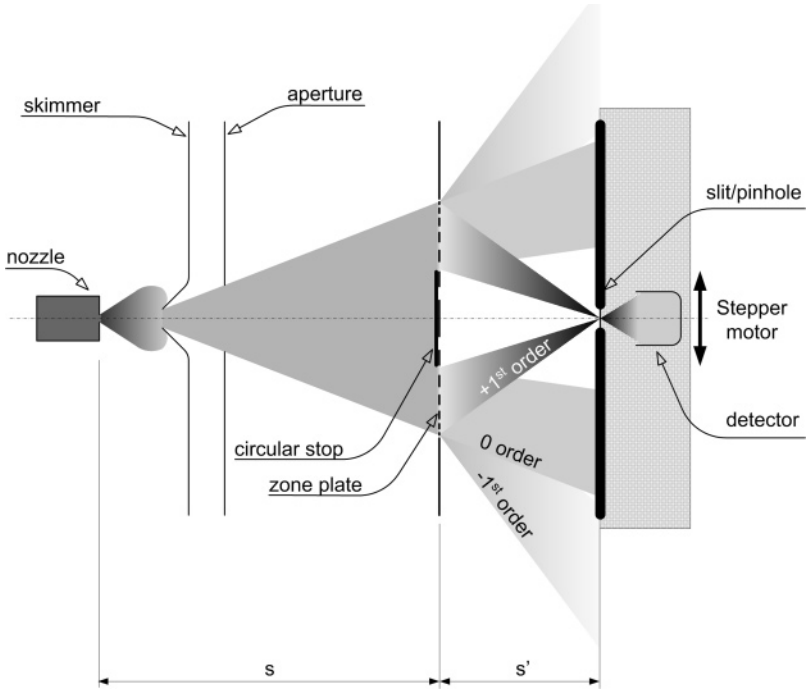


**Figure 2.** Sketch of the experimental setup. The virtual source is taken to be situated in the nozzle plane and imaged by the zone plate's plus first diffraction order onto a slit or a pinhole. The zero as well as the minus first order are also indicated. They contribute to the background signal. $s$ is the distance from the nozzle plane to the zone plate, and $s'$, the distance from zone plate to image plane. The image is recorded by moving the slit or pinhole.

of similar geometry, here referred to as $ZP_1$ and $ZP_2$. In both cases the zone plate was placed $s = 1492$ mm from the source. The whole detector setup was attached to the central part of the apparatus (where the zone plate was placed) by bellows and mounted on a spindle that allowed a variable distance to the zone plate in the range from 680 to 840 mm. In this way the distance $s'$ from the zone plate to the slit/pinhole could be optimized to place the slit/pinhole in the image plane. Given the distribution of the rings on the zone plate and the wavelength of the beam, the expected focal length $f = 506$ mm could be calculated (the same for both zone plates), giving an expected image distance of $s' = 765$ mm (taking the nozzle plane to be the source plane). Experimentally, the optimum image position was found at $s' = 766 \pm 3$ mm (using a microskimmer, see ref 15). In principle, the location of the image plane differs slightly for the different pressures because the virtual-source plane moves away from the nozzle as the pressure increases. This effect, however, is so small that it could not be observed in these experiments and all measurements presented here were carried out at the same image position. The zone plate acts as a lens and the obtained image scans must be corrected by the demagnification factor $M = s'/s = 0.513$ to obtain the true virtual-source size.

## 3. Theoretical Model

As discussed in the Introduction the supersonic expansion of a gas through a nozzle of diameter $d_{nz}$ is a complex process in which interatomic collisions play a fundamental role. During the expansion the temperature of the gas is reduced and its random thermal energy in the source is converted into the beam translational kinetic energy. The velocity distribution of the atoms, $f(\vec{v})$, narrows until the collision frequency is negligible. In the proximity of the nozzle the collisions are very frequent, but as the beam expands, the gas density decreases and thereby the collision frequency also decreases. Beyond a certain distance the frequency is so low that the collisions can be neglected. In the so-called sudden freeze model the flow is approximated by two regimes. Up to a certain distance the flow is approximated as a continuum flow and then at the so-called quitting surface it is assumed that no more collisions take place and molecular flow sets in. In practice, there will be a so-called "quasi molecular flow regime" between the continuum and molecular flow, but this regime is neglected in the model.

In the sudden freeze model the evolution of $f(\vec{v})$ during the expansion can be calculated by means of the Boltzmann equation that is solved using the approximate method discussed in refs 28 and 29 that is suitably adapted for the present case. The first basic assumption is to treat the beam expansion beyond the nozzle as spherically symmetric so that the flow properties depend only on the distance from the source. Moreover, to take into account that the velocity components parallel ($v_{||}$) and perpendicular ($v_{\perp}$) to the streamlines behave differently during the expansion, an anisotropic velocity distribution, which is the product of two Maxwellian functions with two temperatures, $T_{||}$ and $T_{\perp}$, respectively, is assumed

$$f(\vec{v}) = n\left(\frac{m}{2\pi k_b T_{||}}\right)^{1/2}\left(\frac{m}{2\pi k_b T_{\perp}}\right) \exp\left(-\frac{m}{2k_b T_{||}}(v_{||} - u)^2 - \frac{m}{2k_b T_{\perp}}v_{\perp}^2\right)$$

where $m$ is the He mass, $k_b$ is the Boltzmann constant, $n$ is the atom density, and $u$ is the most probable velocity of the gas (the flow velocity). The evolution of the parameters $n$, $u$, $T_{||}$, and $T_{\perp}$ with the distance from the source, $z$, is obtained by solving numerically the set of four coupled integro-differential equations derived from the Boltzmann equation using the method of moments:[20]

$$\frac{\mathrm{d}}{\mathrm{d}r}(nur^2) = 0 \qquad r = \frac{z}{d_{\mathrm{nz}}}$$

$$nu\frac{\mathrm{d}u}{\mathrm{d}r} + \frac{\mathrm{d}}{\mathrm{d}r}\left(\frac{nk_{\mathrm{b}}T_{\parallel}}{m}\right) + \frac{2nk_{\mathrm{b}}}{mr}(T_{\parallel} - T_{\perp}) = 0$$

$$\frac{\mathrm{d}}{\mathrm{d}r}\left[u^2 + \left(\frac{3k_{\mathrm{b}}T_{\parallel}}{m}\right) + \left(\frac{2k_{\mathrm{b}}T_{\perp}}{m}\right)\right] = 0$$

$$2nu\frac{\mathrm{d}}{\mathrm{d}r}\frac{k_{\mathrm{b}}T_{\perp}}{m} + \frac{4nu}{r}\frac{k_{\mathrm{b}}T_{\perp}}{m} = \langle \Delta v_{\perp}{}^2 \rangle$$

The first three equations are related to quantities (mass, parallel momentum, and energy) that are conserved during collisions. The last equation is related to the energy associated with the perpendicular motion, $\langle \Delta v_{\perp}{}^2 \rangle$ (the second moment of the perpendicular velocity distribution). It contains the effect of collisions through the collision integral (see below). Note that for clarity the nozzle diameter is referred to as $d_{\mathrm{nz}}$ in the equation above. In the rest of the paper the nozzle diameter is referred to as $d$. The solution is calculated using the standard Runge−Kutta computation procedure.[30] The integration is started at $r = 2.5$ where the spherically symmetric model is found to be a good approximation to describe the expansion.[31] The starting parameters are obtained from the source conditions, $T_0$ and $P_0$, using the analytical formula of ref 32 for the isentropic expanding gas. The distance at which the integration is terminated (distance of the quitting surface $D_{\mathrm{QS}}$) is somewhat arbitrary. A convenient parameter is $\rho_T = T_{\perp}/T_{\parallel}$, which is a measure for the collisional coupling among the beam atoms. Within the source, where the gas is in equilibrium, $\rho_T = 1$, and in the molecular flow regime $T_{\perp}$ monotonically decreases to zero because of geometrical effects and $T_{\parallel}$ levels off; therefore $\rho_T \rightarrow 0$ for $r \rightarrow \infty$. In the calculations presented here we assume negligible collisional coupling at $\rho_T \leq 0.01$. Stopping the integration at $\rho_T = 0.005$ alters the calculation results less than 0.1%. Values of physical parameters, such as the speed ratio $S = \sqrt{1/2mu^2/k_bT_{\parallel}}$, are evaluated from the terminal values of the free jet parameters.

The evolution of the velocity distribution is determined by the collision integral

$$\Omega^{(2,1)}(T_{\mathrm{eff}}) = \left(\frac{k_{\mathrm{b}}T_{\mathrm{eff}}}{\pi m}\right)^{(1/2)} \int_0^{\infty} Q^{(2)}(E)\gamma^5 \exp(-\gamma^2)\,\mathrm{d}\gamma$$

$$\gamma = \sqrt{\frac{E}{k_{\mathrm{b}}T_{\mathrm{eff}}}}$$

where $T_{\mathrm{eff}}$ is an effective temperature intermediate to the values of $T_{\perp}$ and $T_{\parallel}$, $Q^{(2)}$ is the cross section, and $E$ is the collision energy of two atoms in the center-of-mass system. We have calculated the scattering cross section and the associated collision integral by taking into account quantum effects that are shown to be quite important for He at temperatures below 10 K.[33] For collisions between Bose−Einstein particles

$$Q^{(2)}(E) = \frac{8\pi\hbar^2}{mE} \sum_{l=0,2,4,\ldots} \frac{(l+1)(l+2)}{(2l+3)} \sin^2(\eta_{l+2} - \eta_l)$$

where $\eta_l$ is the phase shift of the partial wave with orbital angular momentum $l$. Phase shifts are estimated by employing the computation procedure described in detail in ref 34 and the Numerov method[35,36] for the numerical integration of the Schrödinger equation. To describe the He−He interactions, we chose two analytical potentials that were also used in the literature to describe He expansion. The first potential is the well-known Lennard-Jones (LJ) (12-6) potential[37]

$$V^{\mathrm{LJ}}(R) = 4\epsilon\left[\left(\frac{R_0}{R}\right)^{12} - \left(\frac{R_0}{R}\right)^{6}\right]$$

where $R$ is the interatomic distance, $\epsilon = 0.94$ meV is the well depth, and $R_0 = 2.64$ Å is the equilibrium distance.

The second analytical potential is the Hurly and Moldover (HM) potential,[38] which is obtained as the sum of a repulsive term and an attractive contribution in the range $R \geq 0.3$ au, i.e.

$$V^{\mathrm{HM}}(R) = V^{\mathrm{HM}}_{\mathrm{rep}}(R) + V^{\mathrm{HM}}_{\mathrm{disp}}(R)$$

Here

$$V^{\mathrm{HM}}_{\mathrm{rep}}(R) = A \exp(a_1R + a_2R^2 + a_{-1}R^{-1} + a_{-2}R^{-2})$$

where the parameters $A$ and $a_n$ are determined by fitting the potential curve to the *ab initio* results.[39−43] The attractive part is

$$V^{\mathrm{HM}}_{\mathrm{disp}}(R) = -\sum_{n=3}^{8} \frac{g_{2n}(R)\, h_{2n}(R)\, C_{2n}}{R^{2n}}$$

where

$$g_{2n}(R) = 1 - \exp(-bR)\sum_{k=0}^{2n} \frac{(bR)^k}{k!}$$

and the corresponding parameter, $b$, is determined through the comparison with the *ab initio* results. The dispersion coefficients are calculated with the recurrence relation

$$C_{2n} = \Omega_n \left(\frac{C_{2n-2}}{C_{2n-4}}\right)^3 C_{2n-6}$$

where the coefficients $\Omega_n$ are calculated in ref 44 and $C_6 = 1.46097780$ au, $C_8 = 14.117855$ au, and $C_{10} = 183.691250$ au are assumed as starting values.[45] The functions $h_{2n}(R)$ account for relativistic effects and modify the behavior of the dipole−dipole term from $R^{-6}$ to $R^{-7}$ at large $R$. The expression for $h_6$-($R$) is taken from ref 46 and for $n > 3$, $h_{2n}(R) \equiv 1$ is assumed.

The HM potential behaves very similarly to the Tang−Toennies−Liu potential[47] over a wide range of interatomic distances[48] whereas the LJ potential is slightly lower than the HM potential at large $R$; in the repulsive region the LJ curve is the steeper one. The LJ cross section is noticeably smaller than the HM one in the low-energy range ($<10^{-3}$ meV).

Having calculated the velocity distribution of the beam at the quitting surface, one can characterize the virtual source by back-tracing the trajectories to the nozzle plane, which was taken to be the virtual-source plane. We have assumed that the plane of the virtual-source point is located at the nozzle plane because estimations of the distance between the two planes set the position within a fraction of the nozzle diameter,[2,18] which is negligible in comparison to $D_{\mathrm{QS}}$.

Following Beijerinck,[18] the corresponding FWHM of the virtual source has been calculated as

$$d_{\mathrm{B}}^{\mathrm{pot.}} = 2\sqrt{2\ln 2}\,\frac{D_{\mathrm{QS}}\sqrt{k_{\mathrm{b}}T_{\perp}/m}}{u} \qquad (1)$$

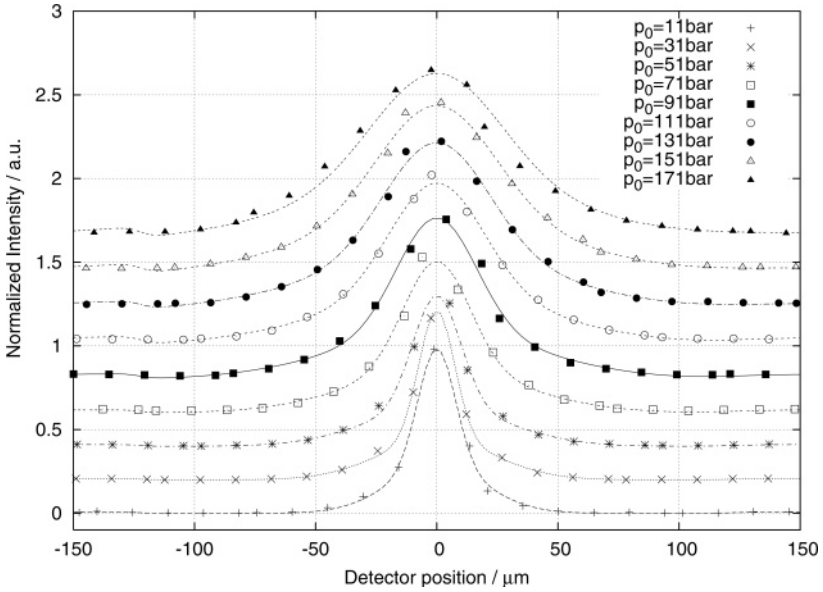


**Figure 3.** Images of the virtual source at different source pressures obtained by stepping a pinhole, 10 $\mu$m in diameter, across the image using zone plate $ZP_2$ to image. The increase in size as a function of pressure can clearly be seen. The data sets have been normalized and fitted with two Gaussian distributions, as explained in the main text.

where "pot." is LJ or HM depending on the potential. The numerical factors transform the dispersion of the Gaussian distribution to FWHM. Unfortunately, this estimation does not represent satisfactorily the data, as will be shown in the next section. On the other hand, the parallel velocity distribution provides a good fit of measured speed ratios;[48] therefore we have modified the model only for the estimation of the perpendicular temperature. Up to the quitting surface, the gas follows approximately a continuum expansion. It has been shown that, for an axisymmetric expansion in the continuum region with $r > 4$, the temperature $T_C$ depends on the distance as[2]

$$T_C(r) = 0.287 T_0 r^{-4/3} \tag{2}$$

Therefore we assume the same scaling with distance for $T_\perp$ and we estimate the virtual-source size as

$$d_C^{\text{pot.}} = 2\sqrt{2 \ln 2}\, \frac{D_{QS}\sqrt{k_b T_C(D_{QS})/m}}{u} \tag{3}$$

where $T_C(D_{QS})$ is the temperature at the quitting surface calculated using eq 2.

## 4. Results

In Figure 3 a series of normalized zone plate focus scans are presented, showing the increase of the virtual-source size with source pressure. The data sets were obtained using $ZP_2$ and stepping across the image with a 10 $\mu$m pinhole. Each data set was fitted with a model based on two Gaussian distributions convoluted with the pinhole transmission function using least-squares minimization. The fitting model also takes into account the higher background signal due to the zeroth-order diffraction and the shadow of the geometrical stop (see Figure 2). In agreement with previous publications[18,25] we find that a model incorporating only a single Gaussian distribution does not yield a good representation of the data. Therefore a model describing the focus with two Gaussian distributions is chosen to represent better the broader tails of the focus. However, we found that allowing the ratio between the two areas of the Gaussian distributions $A_1/A_2$ to vary in the minimization process results in a high dependence on initial parameter values. This may be attributed to the limited resolution of the focus scans, as well as the extension of the Gaussian tails into the zeroth-order region. For this reason the ratio $A_1/A_2$ is fixed to equal 1. This gives an excellent fit of the data, revealing a clear trend in the small and large components of the virtual source (the two Gaussian distributions).

To illustrate the fitting procedure the data set for a nozzle pressure of $p_0 = 51$ bar from Figure 3 is shown on its own in Figure 4 with the two Gaussian components displayed in addition as separate graphs. The raised background due to the zeroth-order diffraction is also visible as well as the dip in intensity due to the shadow of the geometrical stop. Note that data points beyond the zeroth-order diffraction are not included in the fitting procedure.

Additional fits were made for a series of data taken using $ZP_1$ and a vertical slit for stepping across the image to rule out any contributions from imperfections specific to either one of the zone plates. It is known[15] that for both zone plates some zones may be partly blocked by resin left over from the fabrication. This phenomenon is thought to be more pronounced for $ZP_1$. It turned out that the slit scans obtained with $ZP_1$ exhibited a less symmetric image than the pinhole scans obtained with $ZP_2$. This is most likely due to an uneven intensity distribution in the zeroth-order diffraction, caused by partly blocked zones. The virtual-source diameters obtained with $ZP_1$ and $ZP_2$ are shown together in Figure 5. Note that the virtual-source diameters are determined from the zone plate image scans by dividing the FWHM of the two Gaussian distributions by the setup demagnification factor ($M = 0.513$) (see section 2). Also displayed in Figure 5 are results reproduced from ref 25. They will be discussed in section 5. At low pressures both small and large virtual-source diameters of the $ZP_1$ data set are larger than the results from $ZP_2$. We attribute this to the above-mentioned uncertainties with the slit scans. Also the deconvolution of the data sets are more prone to error when the size of the scanned focus is about the same size or smaller than the slit width. For this reason only the results from $ZP_2$ are used in the following analysis.

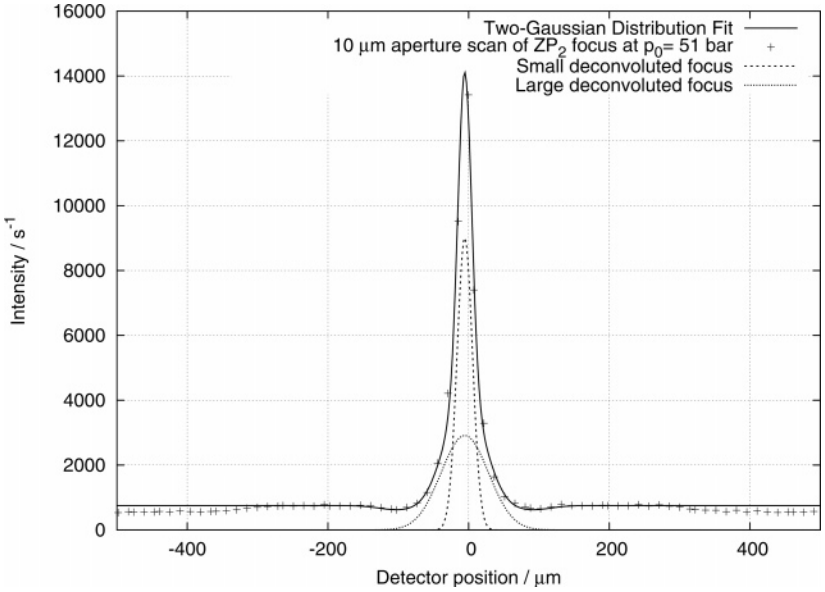


**Figure 4.** Single data set from Figure 3, $p_0 = 51$ bar. The figure illustrates the fitting procedure where two Gaussian distributions are used to fit the data set.

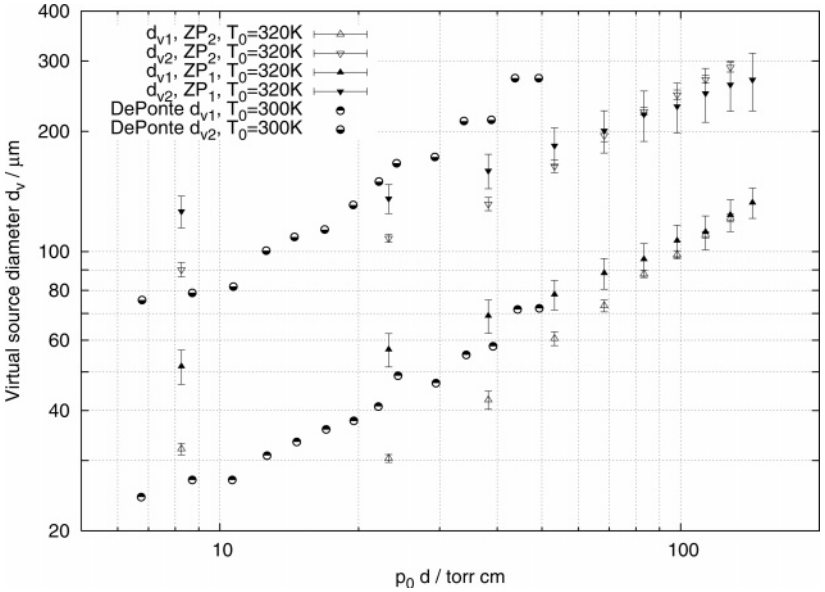


**Figure 5.** Two components of the virtual source $d_{v1}$ and $d_{v2}$ plotted as a function of $p_0d$, where $p_0$ is the source pressure and $d = 10$ $\mu$m is the nozzle diameter. The source temperature $T_0$ is 320 K. Data obtained with two different zone plates are plotted. The $ZP_1$ data were obtained by stepping a slit (25 $\mu$m wide) across the image. The $ZP_2$ data were obtained by stepping a pinhole (10 $\mu$m) across the image. For both zone plate data sets at the smallest $p_0d$ value, enlargement of the virtual-source diameter due to chromatic aberration is significant, whereas it is negligible for the other data points. Also plotted in this figure are data for $d_{v1}$ and $d_{v2}$ from DePonte et al.,[25] obtained with a nozzle diameter 9.5 $\mu$m at a temperature $T_0 = 300$ K.

For low pressures the speed ratio of the helium beam is not sufficiently high to neglect chromatic aberrations. This was determined from another set of focus experiments using a microskimmer and time-of-flight measurements to determine the parallel speed distribution of the beam.[15] The transverse chromatic aberration $\Delta\sigma$ was found to follow theory well, as described by[49]

$$\Delta\sigma \approx 2\sqrt{\ln 2}\, r_N/S \qquad (4)$$

$r_N$ is the radius of the zone plate and $S$ the beam speed ratio. Equation 4 shows that the point spread function due to chromatic aberrations has a FWHM of less than 10 $\mu$m for all data points except $p_0 = 11$ bar, where the contribution due to chromatic aberrations is of the order of the measured focus width. This explains the deviation of this data point from the apparent linear trend in the double-logarithmic graph shown in Figure 5.

In Figure 6 the averages of the small and large virtual-source sizes are plotted corrected for chromatic aberrations. Superimposed as lines are the results of the theoretical calculations detailed in section 3. The direct calculation using either the Lennard-Jones or the Hurly−Moldover potential can be seen to deviate strongly at large $p_0d$. Using a perpendicular temperature at the calculated quitting surface as predicted by a continuum expansion model (see section 3) results in an excellent correspondence to the experiment. A slight preference for the Lennard-Jones potential may be observed. This is not surprising because the Lennard-Jones potential is known to be better at predicting parallel speed ratios at a source temperature of $T_0 = 320$ K.

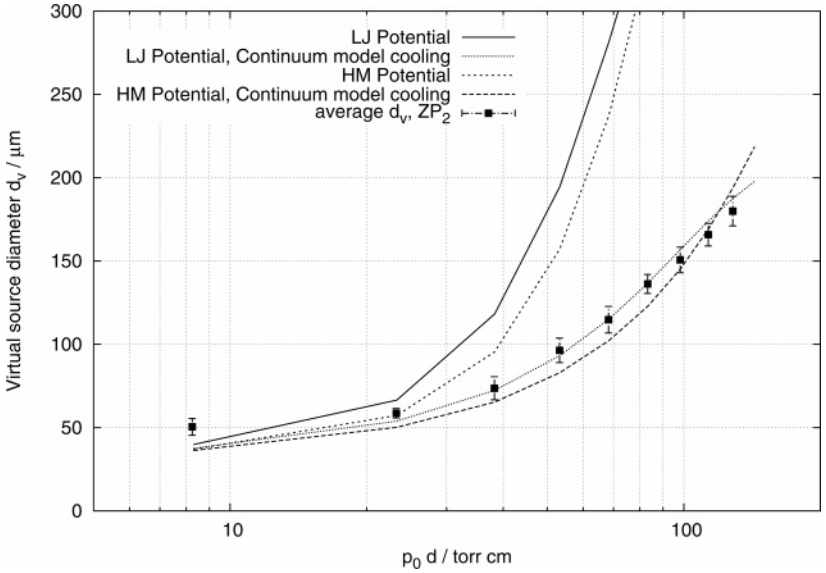


**Figure 6.** Virtual-source diameter $d_v$ obtained as an average of the small and large components as a function of $p_0d$, where $p_0$ is the source pressure and $d = 10$ $\mu$m is the nozzle diameter. The source temperature $T_0$ is 320 K. The data have been obtained using $ZP_2$ by stepping a pinhole (10 $\mu$m) across the image. The data have been corrected for chromatic aberrations. Superimposed as lines are the results of the theoretical calculations. The calculations were only performed for the same $p_0d$ values as in the experiments. The direct calculations using either Lennard-Jones (LJ) or Hurly−Moldover (HM) potential deviate at large $p_0d$. Taking into account a perpendicular temperature at the calculated quitting surface as predicted by a continuum expansion model results in excellent agreement with experiment.

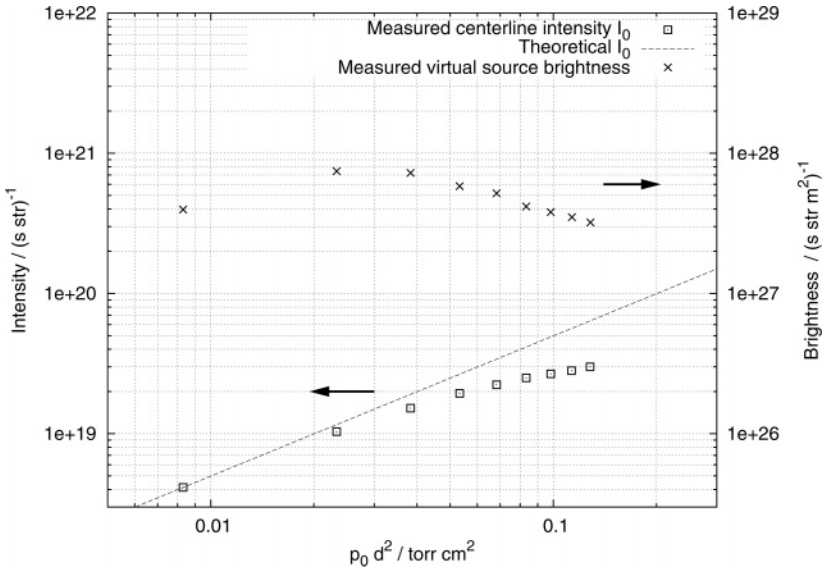


**Figure 7.** Lower data set: center-line intensity measured with the 10 $\mu$m pinhole at 320 K. The line indicates the value predicted for a perfect supersonic expansion. Upper data set: brightness of the source obtained from the maximum intensity in the virtual-source images (see text).

The model sketched above assumes a perfect supersonic expansion. To test if the supersonic expansion in these experiments was really perfect, we measured the center-line intensity as a function of pressure without a zone plate in the beam line. In Figure 7 two data sets are displayed. The lower data set shows the center-line intensity as a function of pressure, obtained by measuring the intensity using the 10 $\mu$m pinhole without the zone plate in the beam line. A drop off from linear dependence is seen at higher pressures. According to theory,[2] the center-line intensity should increase linearly with pressure when the beam is in the molecular flow regime. The drop off at higher pressures, observed in many experimental setups, is most likely due to backscattering from the skimmer.[50] As mentioned earlier we also carried out TOF measurements at various source pressures. The velocity distribution (not shown) is in good agreement with theory[20,51] for all pressures. It has previously been reported that when the backscattering effects are not too pronounced it is possible that center-line intensity is reduced before the velocity distribution is affected.[2]

The upper data set in Figure 7 shows the brightness of the virtual source. The numbers were obtained by measuring the maximum intensity of the zone plate focus using $ZP_2$ with the 10 $\mu$m pinhole. The brightness was then derived by taking into account the scanning hole area, detector efficiency, and transmission efficiency of the zone plate in the first-order focus. The solid angle used to calculate the brightness is given by the area of the zone plate and its distance from the source squared. The brightness is then averaged across the whole virtual source by dividing by a factor of 2. Note that the brightness has a maximum when the center-line intensity starts to deviate from theoretical values.

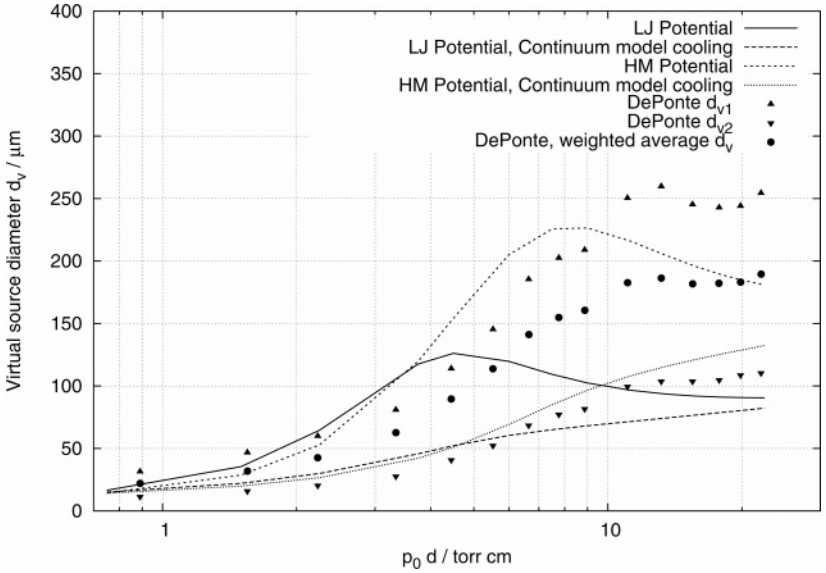


**Figure 8.** Data for the small and broad virtual-source components ($d_{v1}$ and $d_{v2}$) from DePonte at al.[25] obtained at $T_0 = 77$ K and using a 4.3 $\mu$m nozzle, compared with our model. The Lennard-Jones (LJ) potential does not describe the data well although the order of magnitude is correct. The Hurly−Moldover (HM) potential provides a better description.

## 5. Discussion

In Figure 5 the measured virtual-source sizes obtained at $T_0 = 320$ K and with a nozzle diameter of 10 $\mu$m are plotted together with recent data published by DePonte et al.[25] obtained at $T_0 = 300$ K and a nozzle diameter of 9.5 $\mu$m. Taking into account the differences in the two setups and the slightly different temperature, one sees that very similar results are obtained for the size of the smaller virtual-source component, $d_{v1}$. For the larger component of the virtual source, $d_{v2}$, the agreement is not as good. The DePonte data show a steeper increase in source size as a function of pressure. This can be due to various effects. The zone plates have relatively small numerical aperture, and the virtual source is not a perfect extended "light source" in the sense that for a point on the virtual source the atoms do not emerge with equal probability in all directions. This could lead to less intensity being sampled from the edges and hence to a smaller measured source size. A second factor could be the effect of backscattering that could well be different in the two experimental setups.

The results of Figure 7 indicate that in our case the maximum brightness that can be achieved on the central beam axis is not limited by the pressure at which condensation sets in, but rather by the broadening of the virtual source as the pressure increases. This is an important, somewhat unfortunate, implication for experiments using microskimmers, where only a small fraction of the virtual source is selected, because it limits the possible intensity that can be obtained with these microskimmers; i.e., it limits the intensity available for present helium microscope setups where the resolution is determined by the size of the skimmer. Backscattering from the skimmer can affect the beam intensity, as shown by Hedgeland et al.[50] It is possible that backscattering may affect the size of the virtual source, though the good agreement with our model that does not take backscattering into account hints that this is not the case. It is plausible that backscattering affects the overall intensity by removing atoms completely from the beam rather than by broadening the source. It is worth investigating this issue in more detail to improve the performance of helium microscopes. Our measured brightness agrees to within an order of magnitude with the brightness measured by DePonte et al.[25]

Our model allows a quantitative description of the virtual-source size for a supersonic helium expansion at 320 K without any free parameters. To test if the model is able to describe the virtual-source size also in other temperature ranges, we compared the predictions of the model with the results of the virtual-source size measured at 77 K by DePonte et al.[25] both for the smaller and for the larger component of the virtual source. The DePonte data with our fits are shown in Figure 8. The LJ potential does not describe the data well, with either eq 1 or 3, although the order of magnitude is correct. The HM potential provides a better description, especially for the broader component with eq 1 and a good agreement with the smaller component using eq 3. We tried also to compare the predictions with a weighted average of the two sizes using eq 3 and the HM potential. Multiplying by a factor 1.5 gives a good agreement. We conclude that the introduction of the scaling as suggested by the continuum expansion model, eq 3, provides an effective way to predict the size of the virtual source. An obvious improvement of the model would be the direct calculation of the experimental distribution without the need of *ad hoc* assumption of scaling and weighted average. It is worth noting that in the equations $D_{QS}$ seems to be calculated accurately; otherwise, it seems very unlikely that we can get a good agreement with the experiments at different temperatures. We note that the results at 77 and 320 K require different potentials for the best agreement. This was also found for the parallel velocity distribution[48] and does not seem related to the expansion model only but can partially be ascribed to the interaction potentials that are not able to describe the expansion in the whole tested temperature range. In fact, the investigation of a supersonic expansion is a stringent test for both potentials and expansion models because the properties of the gas are probed over several orders of magnitude both for density and for temperature. A complete and consistent description of the expansion process is still lacking. The technique of direct imaging can contribute to gaining further insight in the supersonic expansion process and for measuring interatomic potentials.

## 6. Conclusion

We present first direct images of the virtual source in a supersonic expansion of helium using a Fresnel zone plate to

image the expansion. We show that the virtual-source size increases with pressure. We observe a drop-off from a linear behavior for the center-line intensity at higher pressures which indicates the onset of backscattering effects. This means that we cannot be sure that the broadening of the virtual source in the higher pressure regime is due solely to the effects of a supersonic expansion. New investigations are needed to separate clearly the two effects. In this Article we also propose a new model to analyze the data that shows a good agreement with published data in the source temperature range between 77 and 320 K. The model predicts values for the size of the virtual source through the solution of the Boltzmann equation. The collision integral contains the cross section calculated using realistic potentials; therefore the method of direct imaging of the virtual source can also be applied to test interatomic potentials.

**Acknowledgment.** This work was supported by the European Union FP6, program NEST-Adventure, contract no. 509014, project INA (Imaging with Neutral Atoms).

## References and Notes

(1) *Atomic and Molecular Beam Methods*; Scoles, G., Ed.; Oxford University Press: Oxford, U.K., 1998.
(2) Pauly, H. *Atom, Molecule and Cluster Beams I*; Springer: Berlin, 2002; Vol. 1.
(3) *Atomic and Molecular Beams*; Campargue, R., Ed.; Springer: Berlin, 2001.
(4) Farias, D.; Rieder, K.-H. *Rep. Prog. Phys.* **1998**, *61*, 1575.
(5) Hofmann, F.; Toennies, J. P. *Chem. Rev.* **1996**, *96*, 1307.
(6) *Helium Atom Scattering from Surfaces*; Hulpke, E., Ed.; Springer: New York, 1992.
(7) Chidsey, C. E. D.; Liu, G. Y.; Scoles, G.; Wang, J. *Langmuir* **1990**, *6*, 1804.
(8) Bracco, G.; Acker, J.; Ward, M.; Scoles, G. *Langmuir* **2002**, *18*, 5551.
(9) Rosenbaum, A. W.; Freedman, M.; Sibener, S. J. *J. Phys. Chem. A* **2006**, *110*, 5537.
(10) Ellis, J.; Graham, A. P.; Hofmann, F.; Toennies, J. P. *Phys. Rev. B* **2001**, *63*, 195408.
(11) Pedemonte, L.; Tatarek, R.; Bracco, G. *Phys. Rev. B* **2002**, *66*, 045414.
(12) Druzhinina, V.; DeKieviet, M. *Phys. Rev. Lett.* **2003**, *91*, 193202.
(13) Jardine, A. P.; Dworski, S.; Fouquet, P.; Alesandrowiez, G.; Riley, D. J.; Lee, G. Y. H.; Ellis, J.; Allison, W. *Science* **2004**, *304*, 1790.
(14) Holst, B.; Allison, W. *Nature* **1997**, *390*, 244.
(15) Koch, M.; Rehbein, S.; Schmahl, G.; Bracco, G.; Reisinger, T.; Ernst, W. E.; Holst, B. *J. Microsc.* **2008**, in press.
(16) Doak, R. B.; Grisenti, R. E.; Rehbein, S.; Schmahl, G.; Toennies, J. P.; Wöll, C. *Phys. Rev. Lett.* **1999**, *83*, 4229−4232.
(17) Beijerinck, H. C. W.; Kaashoek, G. H.; Beijers, J. P. M.; Verheijen, M. J. *Physica C* **1983**, *121*, 425.
(18) Beijerinck, H. C. W.; Verster, N. F. *Physica C* **1981**, *111*, 327.
(19) Pauly, H. In *Atomic and Molecular Beam Methods*; Scoles, G., Ed.; Oxford University Press: Oxford, U.K., 1998; Vol. 1.
(20) Toennies, J. P.; Winkelmann, K. *J. Chem. Phys.* **1977**, *66*, 3965.
(21) Klots, C. E. *Chem. Phys.* **1982**, *67*, 75.
(22) Campargue, R. *J. Phys. Chem.* **1984**, *88*, 4466.
(23) Verheijen, M. J.; W. A. R., Beijerinck, H. C. W.; Verster, N. F. *Chem. Phys.* **1984**, *85*, 63.
(24) Beijerinck, H. C. W.; Gerwen, R. J. F. V.; Kerstel, E. R. T.; Martens, J. F. M.; Van Vliembergen, E. J. W.; Smits, M. R. T.; Kaashoek, G. H. *Chem. Phys.* **1985**, *96*, 153.
(25) DePonte, D. P.; Kevan, S. D.; Patton, F. S. *Rev. Sci. Instrum.* **2006**, *77*, 055107.
(26) Apfolter, A. M.Sc. thesis, Institute of Experimental Physics, Technical University, Graz, Austria, 2005.
(27) Rehbein, S. *J. Phys. IV Fr.* **2003**, *104*, 207.
(28) Knuth, E.; Fisher, S. *J. Chem. Phys.* **1968**, *48*, 1674.
(29) Miller, D.; Andres, R. In *VI Symposium of Rarefied Gas Dynamics*; Trilling, L., Wachman, H., Eds.; Academic: New York, 1969; Vol. 2, p 1385.
(30) Mikhlin, S.; Smolitsky, K. In *Approximate Methods for Solution of Differential and Integral Equations*; Bellman, R., Kalaba, R., Eds.; American Elsevier: New York, 1967.
(31) Ashkenas, H.; Sherman, F. In *V Symposium of Rarefied Gas Dynamics*; de Leeuw, J., Ed.; Academic: New York, 1966; Vol. 2, p 84.
(32) Murphy, H.; Miller, D. *J. Chem. Phys.* **1984**, *88*, 4474.
(33) Imam-Rahajoe, S.; Curtiss, C.; Bernstein, R. *J. Chem. Phys.* **1965**, *42*, 530.
(34) Bernstein, R. *J. Chem. Phys.* **1960**, *33*, 795.
(35) Johnson, B. *J. Chem. Phys.* **1977**, *67*, 4086.
(36) Gonzalez, J. Q.; Thompson, D. *Comput. Phys.* **1997**, *11*, 514.
(37) Toennies, J. *Chem. Phys. Lett.* **1973**, *20*, 238.
(38) Hurly, J.; Moldover, M. *J. Res. Natl. Inst. Stand. Technol.* **2000**, *105*, 667.
(39) Ceperley, D.; Partridge, H. *J. Chem. Phys.* **1986**, *84*, 820.
(40) Korona, T.; Williams, H.; Bukowski, R.; Jeziorski, B.; Szalewicz, K. *J. Chem. Phys.* **1997**, *106*, 5109.
(41) Komasa, J. *J. Chem. Phys.* **1999**, *110*, 7909.
(42) Van de Bovenkamp, J.; van Duijneveldt, F. *J. Chem. Phys.* **1999**, *110*, 11141.
(43) van Mourik, T.; Dunning, T., Jr. *J. Chem. Phys.* **1999**, *111*, 9248, and references therein.
(44) Thakkar, A. *J. Chem. Phys* **1988**, *89*, 2092.
(45) Bishop, D.; Pipin, J. *Int. J. Quantum. Chem.* **1993**, *45*, 349.
(46) Jamieson, J.; Drake, G.; Dalgarno, A. *Phys. Rev. A* **1995**, *51*, 3358.
(47) Tang, K.; Toennies, J.; Yiu, C. *Phys. Rev. Lett.* **1995**, *74*, 1546.
(48) Pedemonte, L.; Bracco, G. *J. Chem. Phys.* **2003**, *119*, 1433.
(49) Michette, A. G. *Optical Systems for Soft X-rays*; Plenum Press: New York, 1986.
(50) Hedgeland, H.; Jardine, A. P.; Allison, W.; Ellis, J. *Rev. Sci. Instrum.* **2005**, *76*, 123111.
(51) Miller, D. In *Atomic and Molecular Beam Methods*; Scoles, G., Ed.; Oxford University Press: Oxford, U.K., 1998; Vol. 1, p 14.